Appendix A. Supplementary data

Engineering Oxygen Vacancies in CoO@Co_3O_4/C Nanocomposites for Enhanced Electrochemical Performances

Hongqi Chu [a], Dan Zhang [a], Panpan Feng [a], Yulong Gu [a], Pen Chen [b], Kai Pan [b], Haijiao Xie [c], Min Yang [a]*

[a] *MIIT Key Laboratory of Critical Materials Technology for New Energy Conversion and Storage, School of Chemistry and Chemical Engineering, Harbin Institute of Technology, Harbin, 150001, PR China.*

[b] *Key Laboratory of Functional Inorganic Material Chemistry (MOE), School of Chemistry and Materials Science, Heilongjiang University, Harbin, 150080, China.*

[c] *Hangzhou Yanqu Information Technology Co., Ltd, Hangzhou 310003, China.*

*Corresponding author Email: yangmin@hit.edu.cn

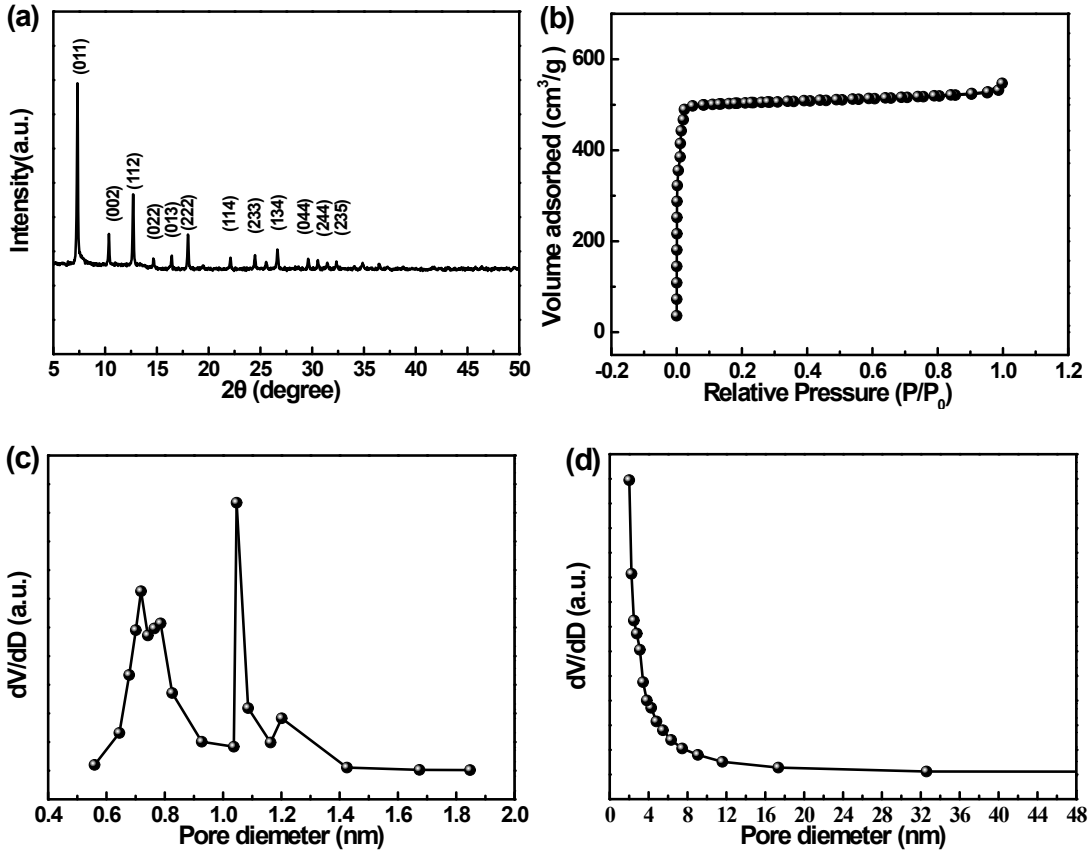

Fig. S1 (a) Powder XRD patterns of as-prepared ZIF-67; (b) Nitrogen adsorption and desorption isotherms for ZIF-67 at 77 K; Pore size distribution plots of ZIF-67: (c) Horvath-Kawazoe (HK) and (d) Barrett-Joyner-Halenda (BJH).

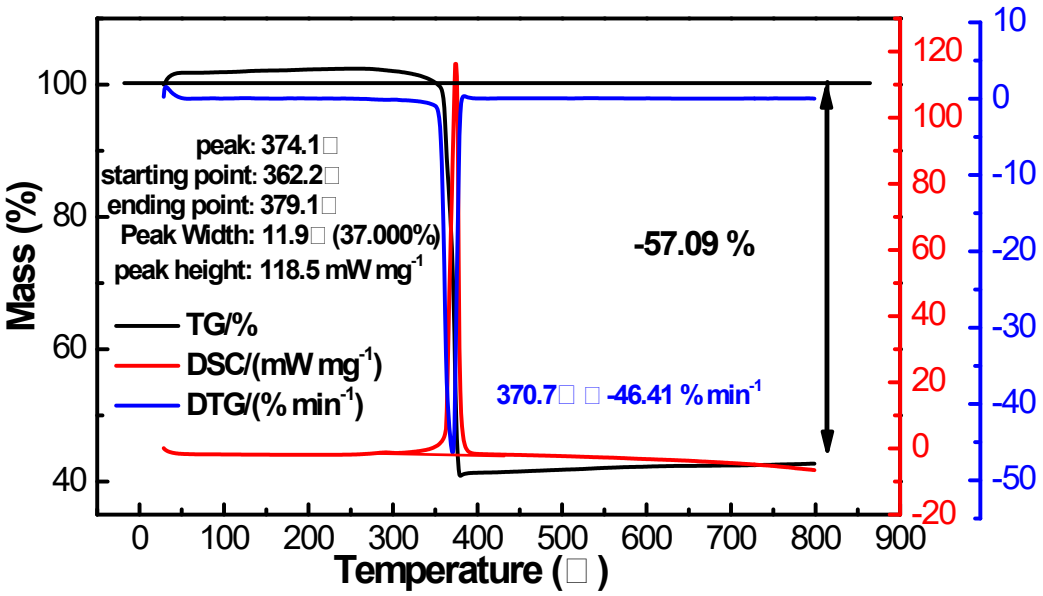

Fig. S2 Thermogravimetric curves of the ZIF-67 precursor.

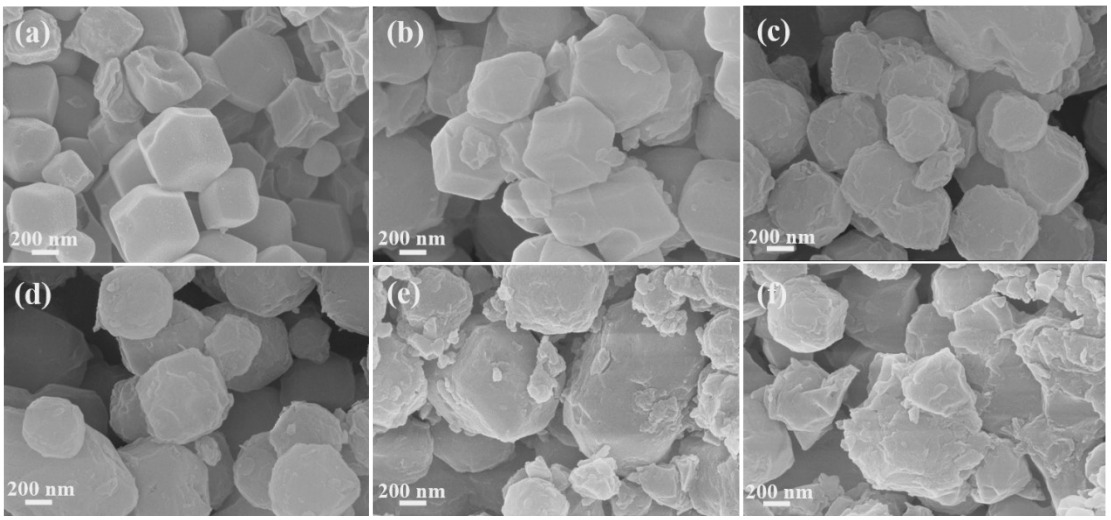

Fig. S3 SEM images of precursors treatment in different glucose concentration: (a) 2 mg mL-

^{1}; (b) 4 mg mL^{-1}; (c) 6 mg mL^{-1}; (d) 8 mg mL^{-1}; (e) 10 mg mL^{-1} and (f) 15 mg mL^{-1}.

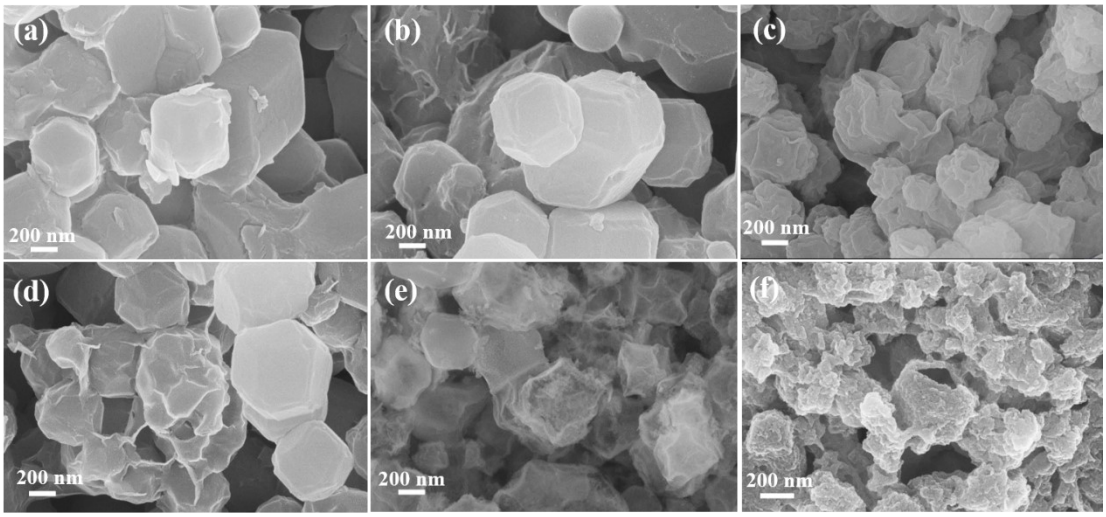

Fig. S4 SEM images of precursors treatment with different vacuum degrees in the heat treatment of Step II: (a) 2.4 mTorr; (b) 0.5 Torr; (c) 10 Torr; (d) 35 Torr; (e) 50 Torr and (f) 100 Torr.

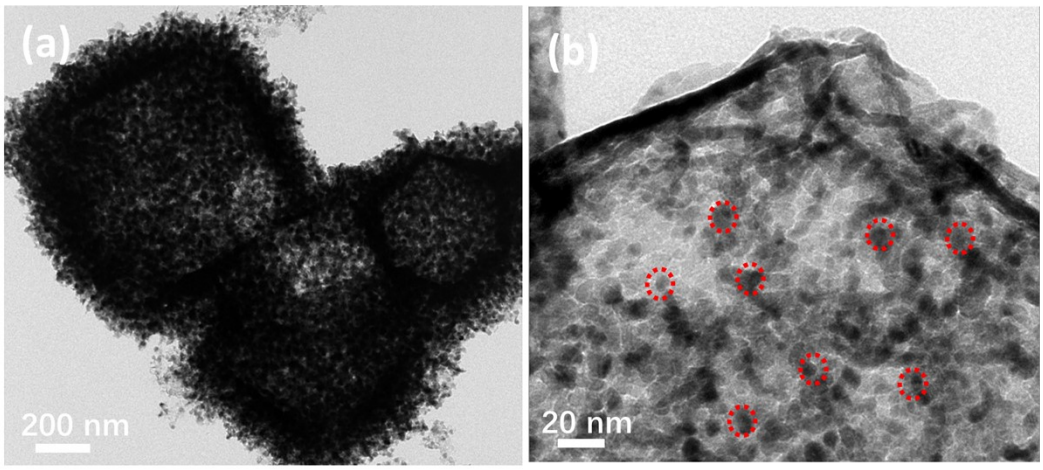

Fig. S5 HRTEM images of (a) CoO@Co_3O_4/C and (b) the precursor after heat treatment in Step II for 0.5 h.

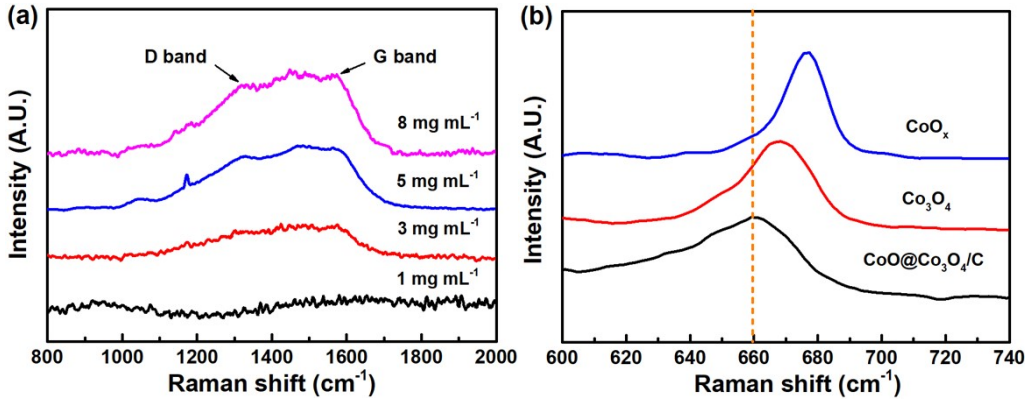

Fig. S6 Raman spectra of (a) precursors treatment in different concentrations of glucose and (b) $CoO@Co_3O_4/C$, CoO_x and Co_3O_4.

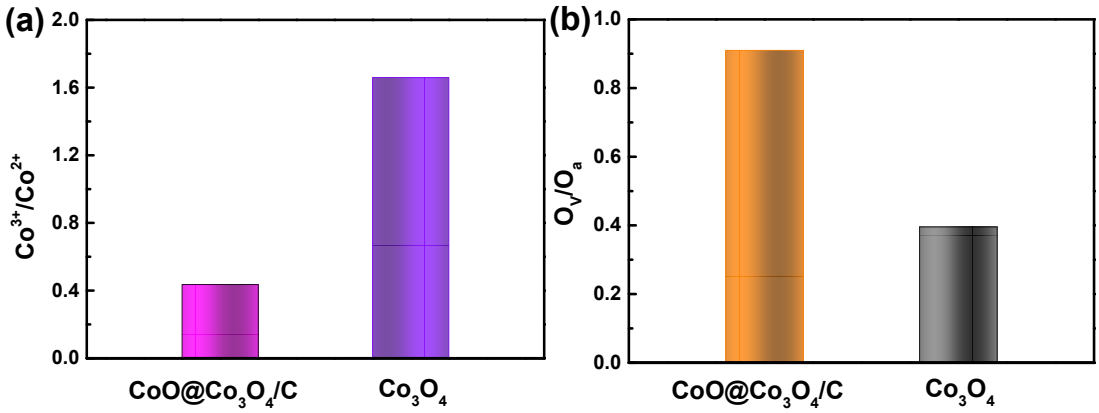

Fig. S7 (a) Co^{3+}/Co^{2+} values of $CoO@Co_3O_4/C$ and Co_3O_4. (b) O_V/O_L values of $CoO@Co_3O_4/C$ and Co_3O_4 obtained from XPS results, this ratio represents the content of oxygen vacancy.

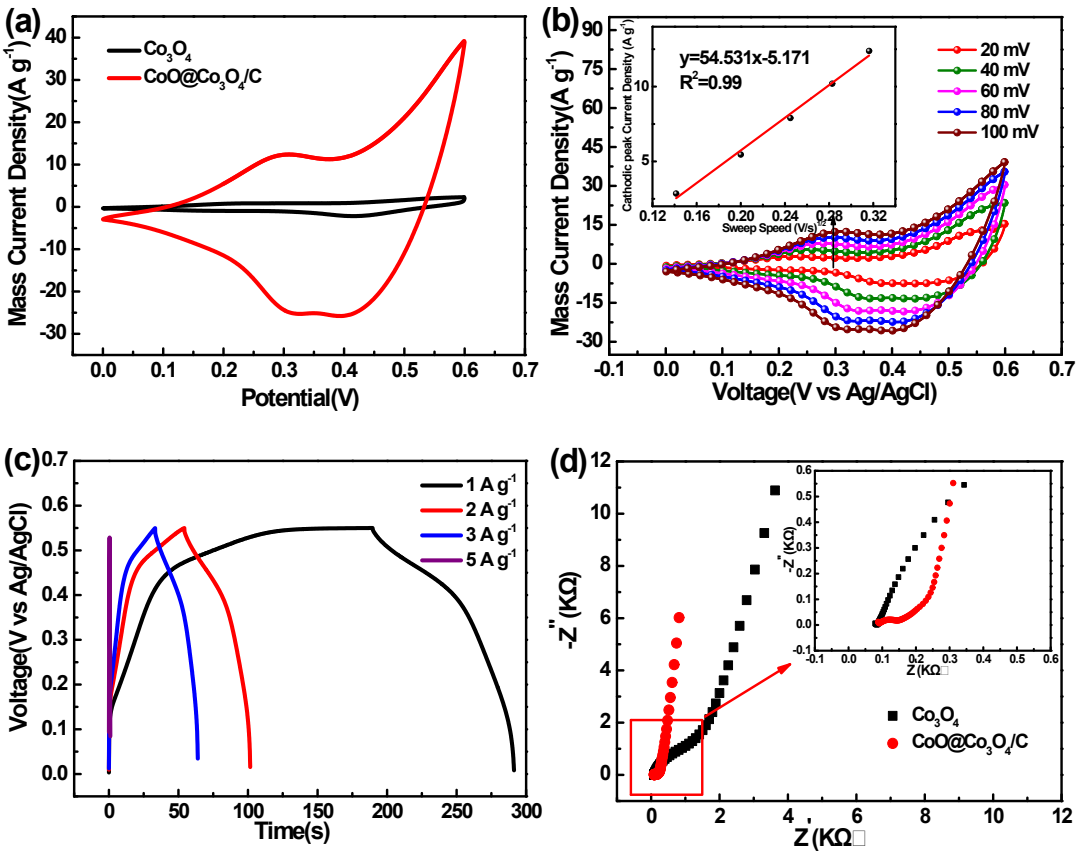

Fig. S8 Electrochemical performance of Co_3O_4 and CoO@Co_3O_4/C: (a) CV curves with scan rate of 100 mV s^{-1}; (b) CV curves of CoO@Co_3O_4/C with different scan rate between 10 and 100 mV mVs^{-1} (insert is diagram of the square root of anodic peak current and scanning rate); (c) Galvanostatic charge/discharge curves of CoO@Co_3O_4/C with different current densities from 1 to 5 A g^{-1}; (d) EIS Nyquist plots of Co_3O_4 and CoO@Co_3O_4/C.

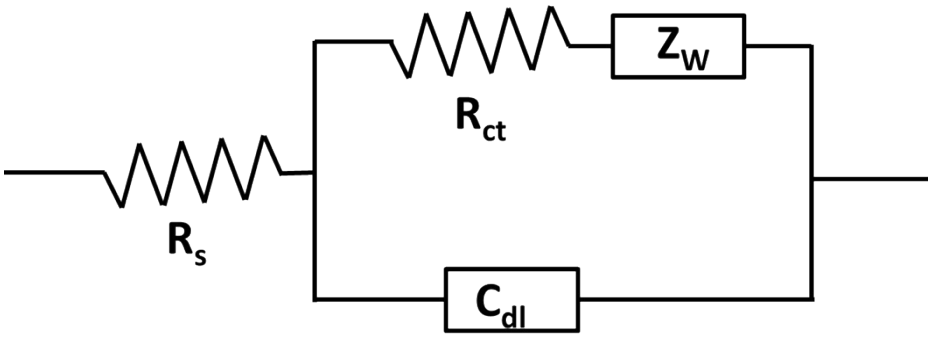

Fig. S9 Equivalent circuit diagram of Co_3O_4 and $CoO@Co_3O_4/C$.

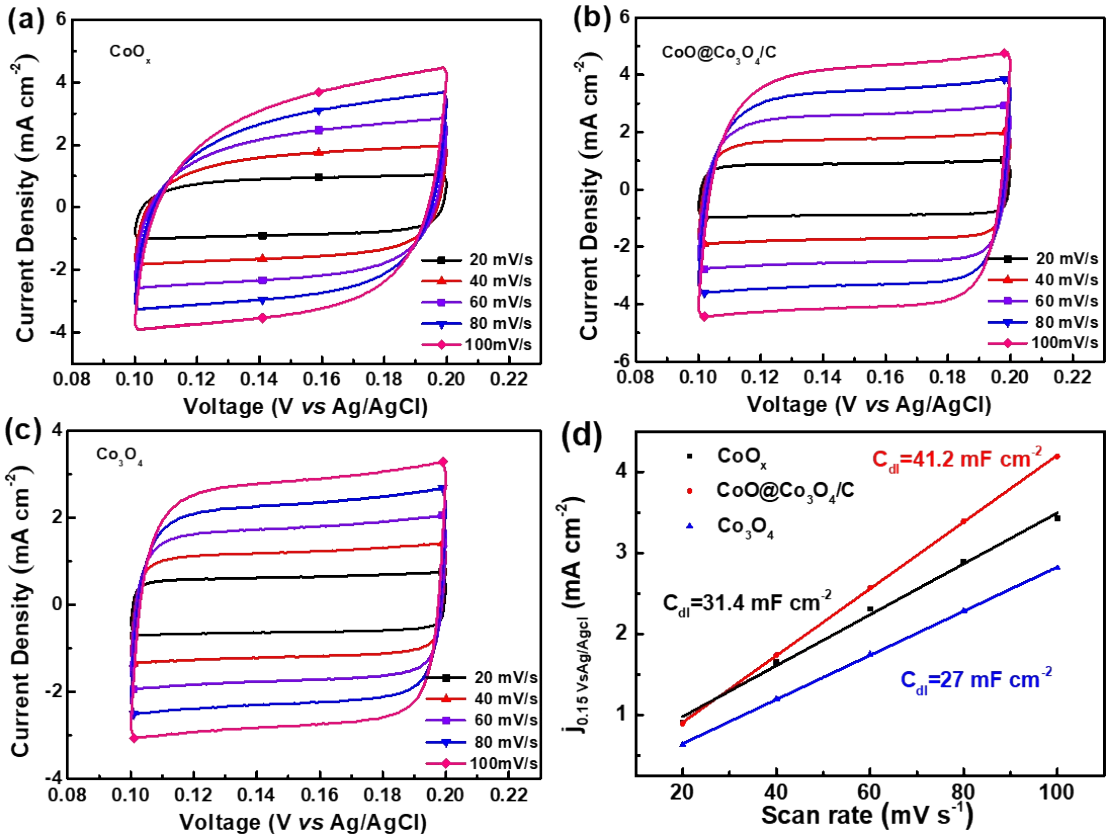

Fig. S10 Electrochemical measurements of the double-layer capacitance (C_{dl}) of (a) CoO_x, (b) $CoO@Co_3O_4/C$, and (c) Co_3O_4; (d) plots of the capacitive currents as a function of scan rate for CoO_x, $CoO@Co_3O_4/C$ and Co_3O_4.

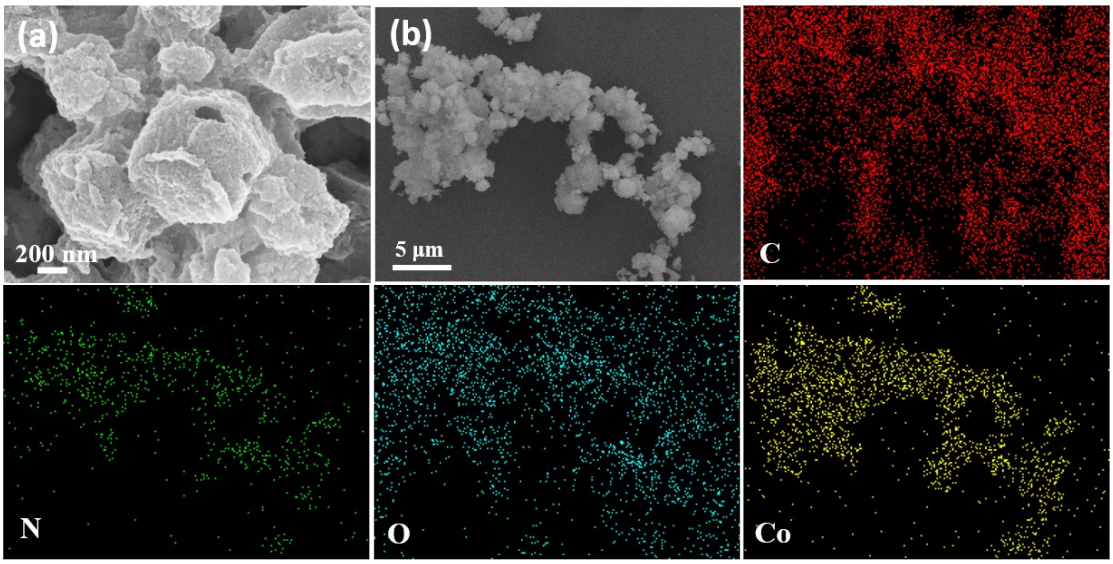

Fig. S11 SEM (a) and elemental mapping images (b) of $CoO@Co_3O_4/C$ after a 30 h stability test in 1 mol L^{-1} KOH.

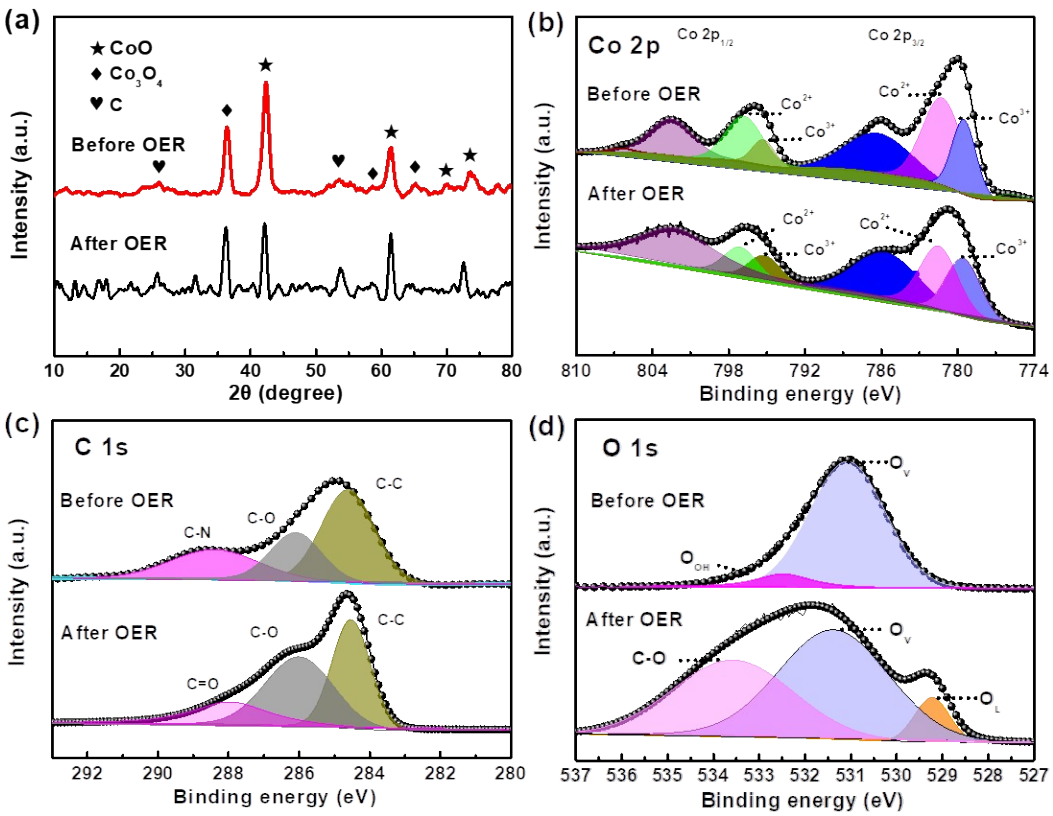

Fig. S12 (a) XRD patterns of CoO@Co_3O_4/C before and after long-time stability test. X-ray photoelectron spectra of CoO@Co_3O_4/C after long-time stability test: (b) Co2p; (c) C1s; (d) O1s; O_v represents the oxygen vacancy; O_L is the lattice oxygen of Co-O; O_{OH} represents the oxygen in hydroxyl arise from physically oxygen species.

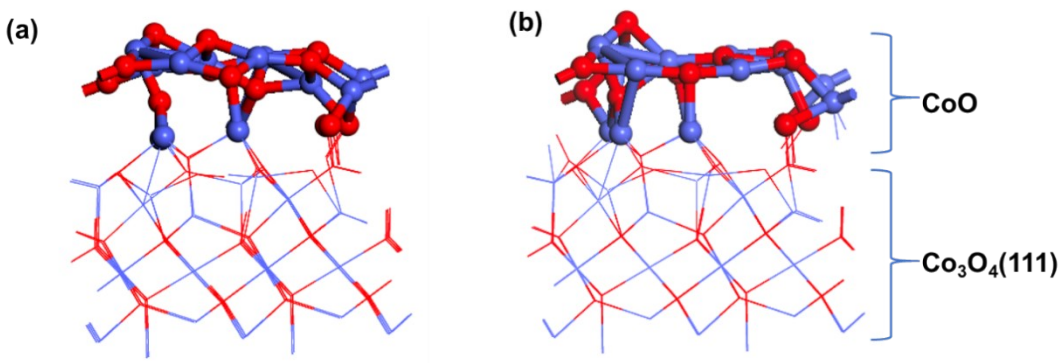

Fig. S13. The optimized structure (side view) of CoO@Co_3O_4/C (a) and CoO@Co_3O_4/C-O-vacancy (b).

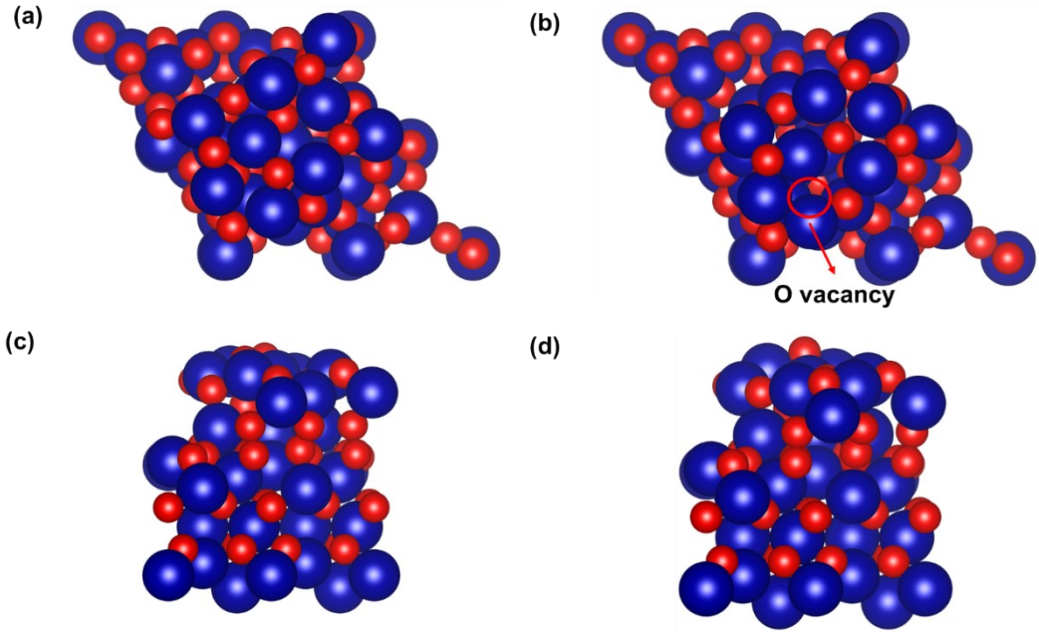

Fig. S14. Vesta display model of CoO@Co_3O_4/C and CoO@Co_3O_4/C-O-vacancy. The optimized structure of (a) CoO@Co_3O_4/C (top view); (b) CoO@Co_3O_4/C-O-

vacancy (top view); (c) CoO@Co_3O_4/C (side view), and (d) CoO@Co_3O_4/C-O-vacancy (side view).

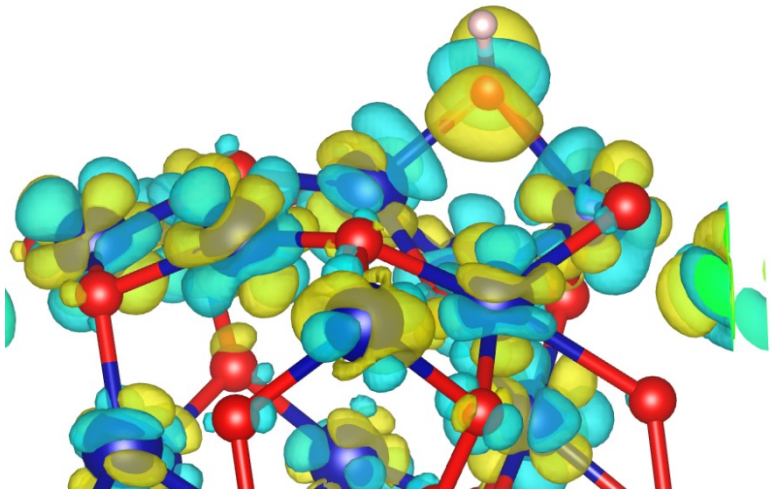

Fig. S15. Charge density difference of $CoO@Co_3O_4/C$ with *OH intermediate, where the isosurface value is set to be 0.01 e/Å and the yellow and cyan refer to the positive and negative charges, respectively.

Table S1. The specific surface area and pore diameter of different samples.

Samples	**ZIF-67**	**CoO_x**	**$CoO@Co_3O_4/C$**	**Co_3O_4**
Specific surface area ($m^2 \cdot g^{-1}$)	1724.8	2311.1	188.5	110.7
Micropore diameter (nm)	1.05	0.72	1.68	1.67
Mesoporous diameter (nm)	/	2.8	3.97	3.14

Table S2. Comparison of OER activity for $CoO@Co_3O_4/C$ and recently reported Co-based catalysts.

Catalyst	Loading density (mg cm^{-2})	Overpotential at 10 mA cm^{-2} (mV)	Tafel slope (mV dec^{-1})	Substrate	Reference
$CoO@Co_3O_4/C$	**0.269**	**287**	**75**	**Glassy carbon**	**This work**
$Co_2Mo_3O_8$@ NC-800	0.14	331	87.5	Glassy carbon	*Angew. Chem. Int. Ed.* **2020**, 59(29): 11948-11957
Pd-e-NiCo-PBA-C	0.28	309	67	Glassy carbon	*Adv. Funct. Mater,* **2021**, 31(10): 2008989
MXene/Co_3O_4	0.407	300	118	Glassy carbon	*Sci. Bull.,* **2020**, 65(6): 460-466

CoN CoP–TiOx CoP–TiOx CoP–TiOx CoP–TiOx CoP/	0.2	337	72.1	Glassy carbon	*Small,* **2020,** 16(2): 1905075

TiO x					
CoP/TiO_x					
Co_2P/CoNPC	0.39	328	78	Glassy carbon	*Adv. Mater.* **2020,** 32(36): 2003649
Co_3O_4/CeO_2	0.4	270	51.9	Glassy carbon	*Adv. Mater.* **2019**, 31, 1900062
CoSAs-MoS_2/TiN NRs	50	340.6	95.1	Carbon cloth	*Adv. Funct. Mater,* **2021**: 2100233
Co-Mo_2C-CN_x-2	1.048	338	70	Glassy carbon	*Appl. Catal., B: Environ,* **2021**, 284: 119738
$Co_3O_{3.87}F_{0.13}$	0.072	430	56	Glassy carbon	*Appl. Catal., B: Environ,* **2021**, 281: 119535
PdCo-300	0.455	350	50	Glassy carbon	*Appl. Catal., B: Environ,* **2019**, 243: 175-182
Co_3O_{4-x}	1.5	309	88	Nickel foam	*J. Catal,* **2020**, 381: 395-401
CoP/NCNHP	0.39	310	70	Glassy carbon	*J. Am. Chem. Soc.* **2018**, *140*, 2610−2618
3D $CoS_{0.46}P_{0.54}$	0.354	302	67	Glassy	*Small Methods* **2020**,

				carbon	4(7): 2000043
Co–MoO$_x$	0.28	340	49	Carbon cloth	*J. Mater. Chem. A,* **2019**, 7, 1005